Estimate (10) is asymptotically valid for a very porous polymer layer. The exponent in the power-law relation between the response time τ_{diff} and thickness h deviates from 2 by the fractal dimension d_{fr} because of the presence of the fractal pores in the polymer layer. Relation (10) provides an explanation for the experimental finding that the exponent q in the power-law relation $\tau_{\text{diff}} \propto h^q$ is less than 2 for porous PSPs.[7,8] Also, this relation can serve as a useful tool to extract the fractal dimension of the tubelike pores in a very porous polymer layer from measurements of the diffusion response time. The fractal dimension d_{fr} of the pore in the polymer poly(TMSP) is $d_{fr} = 1.71$. For the GP197/BaSO4 mixture, the fractal dimension d_{fr} is close to 1. In addition, based on the experimental results shown in Fig. 2, one knows that the fractal dimension d_{fr} for the polymer poly(TMSP) linearly decreases with temperature in a temperature range from 293.1 to 323.1 K. This implies that the geometric structure of the pore in poly(TMSP) may be altered by temperature change. Note that the diffusivity D_m of oxygen mass transfer is also temperature dependent, but it is independent of the coating thickness h. Therefore, the experimental results in Fig. 2 mainly reflect the effect of temperature on the geometric structure of the pores in the polymer rather than the diffusivity.

Conclusions

The Note develops a simple phenomenological model for the effective diffusivity of a porous PSP and gives a new expression that clearly illustrates the relationship between the diffusion timescale and the fractal dimension of the pores. The theoretical results can not only explain why a porous PSP is able to achieve a very fast time response, but also quantitatively show how the fractal dimension and the parameters of porosity affect the response time. For very porous PSPs, the classical square-law estimate of the diffusion timescale should be replaced by the generalized relation derived in the Note.

References

[1]Carroll, B. F., Abbitt, J. D., Lukas, E. W., and Morris, M. J., "Step Response of Pressure Sensitive Paints," *AIAA Journal*, Vol. 34, No. 3, 1996, pp. 521–526.

[2]Winslow, N. A., Carroll, B. F., and Kurdila, A. J., "Model Development and Analysis of the Dynamics of Pressure-Sensitive Paints," *AIAA Journal*, Vol. 39, No. 4, 2001, pp. 660–666.

[3]Fonov, S., Mosharove, V., Radchenko, V., Engler, R., and Klein, C., "Application of the PSP for Investigation of the Oscillating Pressure Fields," AIAA Paper 98-2503, June 1998.

[4]Carslaw, H. S., and Jaeger, J. C., *Conduction of Heat in Solids*, 2nd ed., Oxford Science, Oxford, 2000, Chap. 12.

[5]Crank, J., *The Mathematics of Diffusion*, 2nd ed., Oxford Science, Oxford, 1995, Chap. 2.

[6]Sakaue, H., Gregory, J. W., Sullivan, J. P., and Raghu, S., "Porous Pressure-Sensitive Paint for Characterizing Unsteady Flowfields," *AIAA Journal* (to be published).

[7]Teduka, N., "Fast Response Pressure Sensitive Coatings for Unsteady Measurements," M.S. Thesis, Dept. of Mechanical Systems Engineering, Tokyo Univ. of Agriculture and Technology, Tokyo, April 2001.

[8]Asai, K., Nakakita, K., Kameda, M., and Teduka, N., "Recent Topics in Fast-Responding Pressure-Sensitive Paint Technology at National Aerospace Laboratory," 19th International Congress on Instrumentation in Aerospace Simulation Facilities (ICIASF), Aug. 2001, pp. 25–36.

[9]Mandelbrot, B. B., *The Fractal Geometry of Nature*, W. H. Freeman, New York, 1982, Chap. 4.

[10]Nishimoto, K., *Fractional Calculus*, Descartes, Koriyama, Japan, 1991, Chap. 1.

[11]Cunningham, R. E., and Williams, R. J. J., *Diffusion in Gases and Porous Media*, Plenum, New York, 1980, Chap. 1.

[12]Neogi, P., "Transport Phenomena in Polymer Membranes," *Diffusion in Polymers*, edited by P. Neogi, Marcel Dekker, New York, 1996, Chap. 4.

R. P. Lucht
Associate Editor

Evaluation of Turbulence-Model Performance in Jet Flows

S. L. Woodruff*
Florida State University, Tallahassee, Florida 32306-4120
J. M. Seiner†
University of Mississippi, University, Mississippi 38677
and
M. Y. Hussaini‡ and G. Erlebacher§
Florida State University, Tallahassee, Florida 32306-4120

Introduction

THE importance of reducing jet noise in both commercial and military aircraft applications has made jet acoustics a significant area of research.[1] A technique for jet-noise prediction commonly employed in practice is the approach of Mani, Gliebe, and Balsa (MGB)[2] based on the Lighthill acoustic analogy.[3] This technique requires as aerodynamic input mean flow quantities and turbulence quantities like the kinetic energy and the dissipation. The purpose of the present Note is to assess existing capabilities for predicting these aerodynamic inputs. Two modern Navier–Stokes flow solvers, coupled with several modern turbulence models, are evaluated by comparison with experiment for their ability to predict mean flow properties in a supersonic jet plume. Potential weaknesses are identified for further investigation. Another comparison with similar intent is discussed by Barber et al.[4] The ultimate goal of this research is to develop a reliable flow solver applicable to the low-noise, propulsion-efficient, nozzle exhaust systems being developed in NASA focused programs. These programs address a broad range of complex nozzle geometries operating in high-temperature, compressible, flows.

Seiner et al.[5] previously discussed the jet configuration examined here. This convergent-divergent nozzle with an exit diameter of 3.6 in. was designed for an exhaust Mach number of 2.0 and a total temperature of 915 K. The acoustic and aerodynamic data reported by Seiner et al.[5] covered a range of jet total temperatures from 40 to 1204 K at the fully expanded nozzle pressure ratio. The aerodynamic data included centerline mean velocity and total temperature profiles.

Computations were performed independently with two computational fluid dynamics (CFD) codes, ISAAC[6] and PAB3D.[7] Turbulence models employed include the k–ε model,[8] the Gatski–Speziale algebraic-stress model,[9] and the Girimaji model,[10] with and without the Sarkar compressibility correction.[11] Centerline values of mean velocity and mean temperature are compared with experimental data.

Codes and Models

ISAAC (Integrated Solution Algorithm for Arbitrary Configurations)[6] is a finite volume code of second-order accuracy, which solves the full Favre-averaged Navier–Stokes equations. An upwind scheme based on Roe's flux splitting is used for the convective terms, central differencing for the diffusion terms, and an implicit, spatially split, approximate-factorization scheme for iteration.

Received 2 February 1999; revision received 18 December 1999; accepted for publication 26 February 2000.

*Assistant Scientist, Center for Advanced Power Systems.
†Professor, National Center for Physical Acoustics.
‡Professor, School of Computational Science and Information Technology.
§Professor, Department of Mathematics and School of Computational Science and Information Technology.

The PAB3D code[7] solves the Reynolds-averaged Navier–Stokes equations in a thin-shear-layer approximation. Diffusion terms are central differenced. The implicit iteration operator employs the van Leer scheme, and the explicit terms (e.g., convective terms) are evaluated with the Roe scheme.

The grid used here is composed of five blocks: one in the nozzle (61×61 mesh points), one external to the nozzle (61×61 mesh points), and three blocks downstream of the nozzle exit (65×121, 97×121, and 97×121 mesh points). The mesh is very fine near the nozzle walls and near the jet axis in the plume and becomes gradually coarser away from the axis. Grid-independence tests (see later in this section) indicated this grid was adequate for the computations of the quantities examined in this work. Velocity, pressure, and temperature boundary conditions consistent with experimental conditions are imposed at the upstream boundary inside the nozzle, and a modest freestream flow of $M = 0.05$ is imposed through a one-dimensional characteristic far-field boundary condition at all nonwall boundaries except the downstream boundary, where a subsonic outflow boundary condition is imposed. No-slip boundary conditions are imposed at all walls, and axisymmetry is assumed.

The turbulence models employed in this investigation include both k–ε and algebraic-stress two-equation models. The Reynolds stress τ_{ij} is modeled by the expression

$$\bar{\rho}\tau_{ij} = \tfrac{2}{3}\bar{\rho}k\delta_{ij} - 2\bar{\rho}C^*_\mu f_\mu\left(k^2/\varepsilon_s\right)\left[\left(S_{ij} - \tfrac{1}{3}S_{kk}\delta_{ij}\right) + \alpha_4(k/\varepsilon_s)(S_{ik}W_{kj} + S_{jk}W_{ki}) - \alpha_5(k/\varepsilon_s)\left(S_{ik}S_{kj} - \tfrac{1}{3}S_{kl}S_{kl}\delta_{ij}\right)\right] \quad (1)$$

where $S_{ij} = (\frac{1}{2})(\tilde{u}_{i,j} + \tilde{u}_{j,i})$ and $W_{ij} = (\frac{1}{2})(\tilde{u}_{i,j} - \tilde{u}_{j,i})$ are the symmetric and antisymmetric parts of the mean-velocity-gradient tensor. Commas denote differentiation, $\tilde{u}_i$ are velocity components, and $\bar{\rho}$ is the average density. The remaining symbols are defined next.

The turbulent kinetic energy k and the solenoidal part of the dissipation rate ε_s (the total dissipation $\varepsilon = \varepsilon_s + \varepsilon_c$ is the sum of the solenoidal and curl-free dissipations; in the case of no compressibility correction, $\varepsilon_c = 0$) are determined using the conservation equations

$$(\bar{\rho}k)_{,t} + (\bar{\rho}\tilde{u}_j k)_{,j} = -\bar{\rho}\tau_{mn}\tilde{u}_{m,n} - \bar{\rho}\varepsilon + \left\{\left[\mu + \bar{\rho}C^*_\mu f_\mu\left(k^2/\sigma_k\varepsilon_s\right)\right]k_{,j}\right\}_{,j}$$

$$(\bar{\rho}\varepsilon_s)_{,t} + (\bar{\rho}\tilde{u}_j\varepsilon_s)_{,j} = -\bar{\rho}C_{\varepsilon 1}f_1(\varepsilon_s/k)\tau_{mn}\tilde{u}_{m,n} - \bar{\rho}C_{\varepsilon 2}f_2(\varepsilon_s\tilde{\varepsilon}/k) + \left\{\left[\mu + \bar{\rho}C^*_\mu f_\mu\left(k^2/\sigma_\varepsilon\varepsilon_s\right)\varepsilon_{s,j}\right]_{,j}\right\} + \chi_w \quad (2)$$

For the k–ε model $\alpha_4 = 0$, $\alpha_5 = 0$, and $C^*_\mu = C_\mu = \text{const}$. In the k and ε_s equations σ_k, σ_ε, $C_{\varepsilon 1}$, and $C_{\varepsilon 2}$ are constants, and integration to the wall is possible using the damping functions f_μ, f_1, and f_2. Also in the ε equation, we have $\tilde{\varepsilon} = \varepsilon_s - \mu/\rho|\nabla\sqrt{k}|^2$ and χ_w, a wall-correction function.

The Gatski–Speziale algebraic-stress model[9] employs Eq. (1) with C^*_μ, α_4, and α_5 functions of k, ε, and invariants of S_{ij} and W_{ij}. No wall damping of the Reynolds stress is required so that $f_\mu = 0$, and in ISAAC new f_1 and f_2 are introduced to preserve proper log-law behavior.

The Girimaji algebraic-stress model[10] also employs Eq. (1); in this case the coefficients C^*_μ, α_4, and α_5 are determined via the (explicit) solution of a cubic algebraic equation see the work of Girimaji[10] for details of this solution and of the selection of the physically relevant root.

The models were tested both with and without the Sarkar compressibility correction,[11] which gives for the compressible part of the turbulent dissipation ε_c the value $\alpha_c M_t^2 \varepsilon_s$, M_t being the turbulent Mach number $\sqrt{\tau_{ii}}/a_\infty$ and α being a constant taken here to be 0.5.

Results and Discussion

Computations were performed at jet total temperatures of 40 and 843 K. Extensive tests of the adequacy of the spatial resolution were conducted; comparison of runs with the full grid and with the grid coarsened by factors of 2 and 3 showed negligible differences. The value of y^+ for points adjacent to the walls of the nozzle was always less than 0.5 for the full-resolution computation, indicating that the wall layers were satisfactorily resolved. All runs were continued well past the point where a steady state in the mean quantities had been reached.

Data for the 843 K case appear in Fig. 1. The mean velocity and temperature at the centerline are shown as computed using the various models discussed in the preceding section and compared with experimental results.[5] Although there is a good deal of variation in the computational results (this variation is much greater than the experimental uncertainty[5]), the ISAAC results are better, overall, than the PAB3D results. The centerline mean velocity for the 40 K case is shown (model by model) in Figs. 2 and 3, and agreement

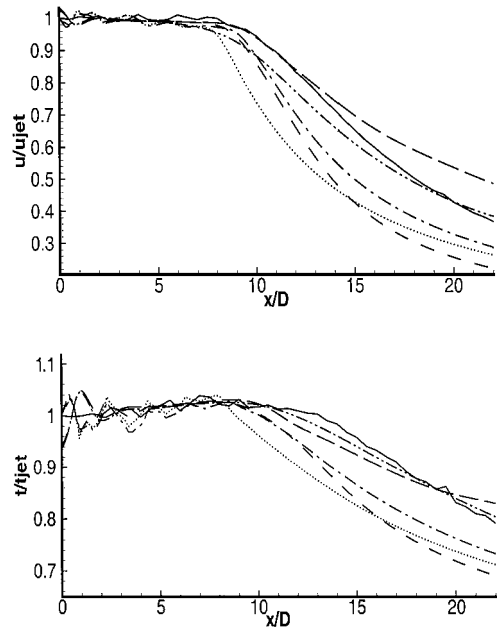

Fig. 1 No compressibility correction, 843 K case: ——, experiment; –···–, ISAAC k–ε model; ——, ISAAC GS ASM; . . . ., PAB3D k–ε model; –·–, PAB3D GS ASM; and – – –, PAB3D Girimaji ASM.

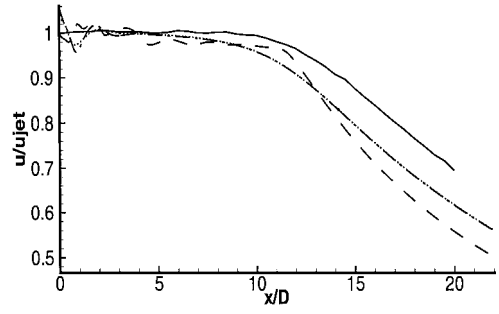

Fig. 2 Comparison of k–ε models, 40 K case: ——, experiment; –·–, ISAAC; – – –, PAB3D; and . . . ., PAB3D model in ISAAC.

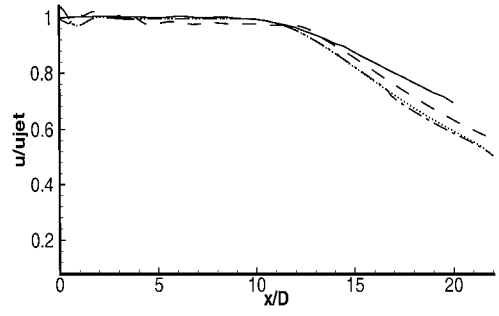

Fig. 3 Comparison of Gatski–Speziale ASMs, 40 K case: ——, experiment; –·–, ISAAC; – – –, PAB3D; and . . . ., PAB3D model in ISAAC.

is fairly good for both codes. Although the results shown here are worse than one would like, they are better than earlier results.[4]

The simulations employing the Sarkar compressibility correction were generally no better than those not. In the 40 K jet case the correction makes the PAB3D predictions significantly worse, and the ISAAC predictions are slightly high by about as much as they were low for the computations without the compressibility correction. In the 843 K jet case the compressibility correction significantly improves the PAB3D results but makes the ISAAC results dramatically worse.

Figure 1 shows a grouping of the results from each of the two codes; this grouping occurred in the other case as well. It suggests the differences in results can be caused more by differences in the codes than to differences in the models. To further investigate these differences, the k–ε model in PAB3D was implemented in ISAAC (except for the PAB3D form for χ_w, which involves derivatives not readily available in the ISAAC code), as was the PAB3D implementation of the Gatski–Speziale algebraic stress model (ASM). Comparisons between the ISAAC implementations of the models, the PAB3D implementations of the models, and the PAB3D models implemented in ISAAC are shown in Figs. 2 and 3 for the 40 K case. The results from ISAAC with its own models and with the PAB3D models were very similar for the k–ε model and the Gatski–Speziale algebraic-stress model, indicating that the differences between the ISAAC and PAB3D results are primarily caused by the codes themselves.

Summary

In summary, overall agreement of the computations with experiment is good. The two codes each gave fairly consistent results with the different turbulence models, and the differences between the codes seemed to be greater than the differences between the models. Additional evidence for this was given by the computations with ISAAC using the PAB3D versions of the models, which gave results much closer to the ISAAC results with its own models than to the PAB3D results. Possible reasons for these differences between the results of the two codes include different handling of viscous fluxes (thin shear layer in PAB3D vs full Navier Stokes in ISAAC), first-order advection in the PAB3D turbulence equations vs second-order advection in all equations in ISAAC, and other differences in the numerical algorithms employed in the two codes.

Finally, we note that the aerodynamic input is only part of the story, and the MGB noise prediction can emphasize or deemphasize different aspects of the input error.

Acknowledgments

This work was supported by NASA through the NASA Langley Research Center. The assistance of J. H. Morrison with ISAAC and P. Pao, J. Carlson, and K. S. Abdol-Hamid with PAB3D is gratefully acknowledged. P. Pao and J. Carlson supplied the grid. The ISAAC and PAB3D CFD codes were made available by NASA Langley Research Center.

References

[1]Seiner, J. M., "A New Rational Approach to Jet Noise Reduction," *Theoretical and Computational Fluid Dynamics*, Vol. 10, Nos. 1–4, 1998, pp. 373–383.

[2]Mani, R., Gliebe, P. R., and Balsa, J. F., "High-Velocity Jet Noise Source Location and Reduction," Task 2, Federal Aviation Administration Rept., FAA-RD-76-79-II, 1978.

[3]Lighthill, M. J., "On Sound Generated Aerodynamically. I. General Theory," *Proceedings of the Royal Society of London*, Vol. A211, 1952, pp. 564–587.

[4]Barber, T. J., Chiapetta, L. M., DeBonis, J. R., Georgiadis, N. J., and Yoder, D. A., "Assessment of Parameters Influencing the Prediction of Shear-Layer Mixing," *Journal of Propulsion and Power*, Vol. 15, No. 1, 1999, pp. 45–53.

[5]Seiner, J. M., Ponton, M. K., Jansen, B. J., and Lagen, N., "The Effects of Temperature on Supersonic Jet Noise Emission," AIAA Paper 92-02-046, June 1992.

[6]Morrison, J. H., "A Compressible Navier–Stokes Solver with Two-Equation and Reynolds-Stress Turbulence Closure Models," NASA CR 4440, May 1992.

[7]Abdol-Hamid, K. S., "Implementation of Algebraic-Stress Models in a General 3-D Navier–Stokes Method (PAB3D)," NASA CR 4702, Dec. 1995.

[8]Wilcox, D. C., *Turbulence Modeling for CFD*, DCW Industries, Inc., La Cañada, CA, 1993, Chap. 4.

[9]Gatski, T. B., and Speziale, C. G., "On Explicit Algebraic-Stress Models for Complex Turbulent Flows," *Journal of Fluid Mechanics*, Vol. 254, Sept. 1993, pp. 59–78.

[10]Girimaji, S. S., "Fully-Explicit and Self-Consistent Algebraic Reynolds-Stress Model," Inst. for Computer Applications in Science and Engineering, Rept. 95–82, Hampton, VA, Dec. 1995.

[11]Sarkar, S., Erlebacher, G., Hussaini, M. Y., and Kreiss, H. O., "The Analysis and Modelling of Dilatational Terms in Compressible Turbulence," *Journal of Fluid Mechanics*, Vol. 227, June 1991, pp. 473–493.

P. J. Morris
Associate Editor

Efficient Method for Calculating Wall Proximity

David A. Boger*
Pennsylvania State University,
University Park, Pennsylvania 16804

Introduction

THE problem of calculating the distance to the nearest surface from all of the points throughout a volume mesh is addressed by devising a finite search region and then conducting an efficient geometric search. The method is tested on 10 three-dimensional computational fluid dynamics (CFD) grids with up to 1,700,000 points in the volume and up to 130,000 points on the surface. The expense of the calculation is reduced by orders of magnitude compared to the simplest approach of checking the distance to every surface point. This method is especially useful when the distances need to be updated often, such as multiple-body or moving-appendage problems, and it can be easily retrofitted into existing codes.

Many physical models employed in modern CFD codes require wall proximity in their specification. The most common are low-Reynolds-number turbulence models, many of which rely on wall proximity in near-wall damping functions.[1–3] Researchers have observed that this reliance on explicit wall distance is ambiguous for all but the simplest topologies and that it is "not at all evident that wall distance bears a relationship to the structure of turbulence."[4] As a result, much current research in turbulence modeling is focused on achieving geometry independence.[5,6] The appropriateness of using models that contain wall distance explicitly is not considered here. It is simply observed that such models continue to enjoy widespread use.

For complex geometries the simplest approach, given a point within the volume, is to measure the distance to every point on every solid surface, keeping the minimum. Though simple, this requires $\mathcal{O}(N_v N_s)$ operations, where N_v and N_s are the number of volume and surface points, respectively. In many applications the calculation is performed once and saved, but when the distance function changes with time the efficiency of wall proximity computations can become important. The current note formulates a method for calculating wall proximity with a cost of $\mathcal{O}(N_v \log N_s)$, a gain of several orders of magnitude in the cases shown here.

At least three other methods for computing wall proximity appear in the literature. In the first an approximate distance to the wall was inferred from the solution of a Poisson equation for a length scale L, where $L = 0$ on solid boundaries.[7,8] Described as a "convenient

Received 19 May 2001; revision received 8 July 2001; accepted for publication 13 August 2001.

*Associate Research Engineer, Applied Research Laboratory.